

Meta-Learning Dynamics Forecasting Using Task Inference

Rui Wang ^{*1} Robin Walters ^{*2} Rose Yu ¹

Abstract

Current deep learning models for dynamics forecasting struggle with generalization. They can only forecast in a specific domain and fail when applied to systems with different parameters, external forces, or boundary conditions. We propose a model-based meta-learning method called DyAd which can generalize across heterogeneous domains by partitioning them into separate sub-domains, each with a different task. DyAd has two parts: a prediction network which learns the shared dynamics of the entire domain, and an encoder which infers the parameters of the task. The encoder adapts the prediction network during inference time using adaptive instance normalization and a new layer, AdaPad, specifically designed for boundary conditions. The encoder can also use any weak supervision signals that can help distinguish different tasks, allowing the incorporation of additional domain knowledge. Our model outperforms a variety of state-of-the-art approaches on both turbulent flow and real-world ocean data forecasting tasks.

1. Introduction

Learning dynamical systems with deep neural networks has shown great success in a wide range of systems from fluid mechanics to neural dynamics (Tompson et al., 2017; Chen et al., 2018; Kolter & Manek, 2019; Zoltowski et al., 2020; Li et al., 2021). However, the main limitation of previous work modeling dynamics with neural networks is very limited generalizability. Most approaches treat dynamics data as a time series and train on past data in order to predict future data. Thus a new model must be trained to predict each specific system. It is imperative to develop *generalizable* deep learning models for dynamical systems that can learn and generalize well over a large heterogeneous domain.

^{*}Equal contribution ¹Computer Science and Engineering, University of California San Diego, USA ²Khoury College of Computer Science, Northeastern University, Boston, USA. Correspondence to: Rose Yu <roseyu@eng.ucsd.edu>.

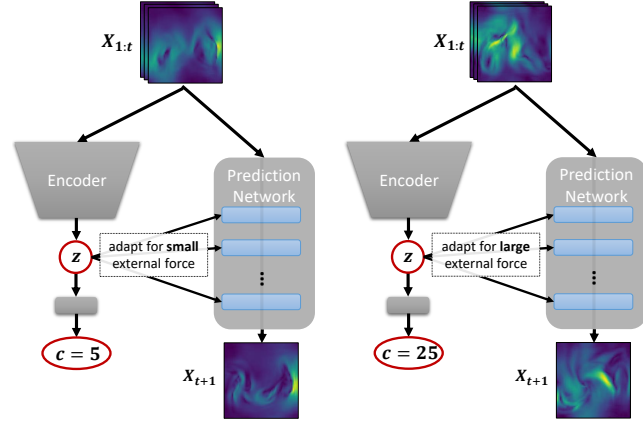


Figure 1. Comparison of DyAd applied to two inputs of fluid turbulence, one with small external forcing and one with larger external forces. The encoder infers the time-shift invariant characteristic variable z which is used to adapt the prediction network.

Meta-learning (Thrun & Pratt, 1998; Baxter, 1998; Finn et al., 2017), or learning to learn, improves generalization by learning multiple tasks from the environment. The recent development in meta-learning has been successfully applied to few-shot classification (Munkhdalai & Yu, 2017), active learning (Yoon et al., 2018), and reinforcement learning (Gupta et al., 2018). However, meta-learning in the context of forecasting high-dimensional physical dynamics has not been studied before. The challenges with meta-learning dynamical systems are unique in that (1) we need to efficiently infer the latent parameters of the dynamical system from observed time series data, and (2) we need to account for changes in unknown initial and boundary conditions.

Our approach is inspired by the fact that similar dynamical systems may share time-invariant characteristic variables. Even the slightest change in these variables may lead to vastly different phenomena. For example, in climate science, fluids are governed by a set of differential equations called Navier-Stokes equations. Some variables such as kinematic viscosity, which measures a fluid's internal resistance to deformation, and external forces, such as gravity, determine the flow characteristics. By inferring these variables, we can model diverse system behavior from smoothly flowing water to atmospheric turbulence.

We propose a model-based meta-learning method, called DyAd, which can rapidly adapt to dynamics systems with different parameters. DyAd has two parts, an encoder g and a prediction network f . The encoder maps different dynamical systems to time-invariant characteristic variables such as constants of motion, boundary conditions, and external forces which vary from system to system. The prediction network f then takes the characteristic variables and the past system states to forecast the future system state. Due to the information in the characteristic variable, the prediction network has the flexibility to adapt to a wide range of systems with heterogeneous dynamics.

Unlike gradient-based meta-learning techniques such as MAML (Finn et al., 2017), DyAd automatically adapts during inference using an encoder and does not require any retraining. Similar to other model-based meta-learning methods such as MetaNets (Munkhdalai & Yu, 2017), we employ a two-part design with an adaptable learner which receives task-specific weights. However, for time series forecasting, since input and output come from the same domain, a support set of additional labeled data is unnecessary to define the task. The encoder can infer the task directly from query input.

Our contributions include:

- A new model-based meta-learning method (DyAd) for forecasting in dynamical systems which adapts to each input using task inference.
- An encoder capable of extracting the time-invariant part of a dynamical system using time-shift invariant model structure and loss.
- A new layer AdaPad designed for boundary conditions.
- Improved accuracy on heterogeneous domains such as fluid flow and sea temperature prediction relative to models trained separately on homogeneous domains or on the entire domain but without task inference.
- Good generalization to new tasks with parameters outside the training distribution.

2. Methods

2.1. Meta-learning in dynamics forecasting

A dynamical system is governed by a set of differential equations:

$$\{\xi^i(\mathbf{x}, \dot{\mathbf{x}}, \ddot{\mathbf{x}}, \dots; \psi) = 0\} \quad (1)$$

where $\mathbf{x} \in \mathbb{R}^d$ is a d -dimensional state of the system and ψ are the parameters. Oftentimes, the dynamics parameter ψ can represent different system coefficients, external forces or boundary conditions.

The problem of dynamics forecasting is that given a set of series from the system in (1), $\{(\mathbf{x}_1, \mathbf{x}_2, \dots, \mathbf{x}_t)^{(i)}\}_{i=1}^n$, we

want to learn a map f such that:

$$f : (\mathbf{x}_{t-l+1}, \dots, \mathbf{x}_t) \longrightarrow (\mathbf{x}_{t+1}, \dots, \mathbf{x}_{t+h}) \quad (2)$$

Here l is the length of the input series and h is the forecasting horizon in the output.

Existing approaches for dynamics forecasting only predict future data for a specific system as a single task. The resulting model often generalizes poorly to different system dynamics. Thus a new model must be trained to predict for systems with different dynamics.

To perform meta-learning, we learn multiple forecasting tasks simultaneously where each task is identified by some parameters $c \subset \psi$, representing time-invariant characteristics such as constants of motion, external forces, and boundary conditions. Here we use c for a subset of parameters because we usually do not have the full knowledge of the system dynamics. The parameters c only partially describe the characteristics in the data.

Consider, for example, the domain of fluid dynamics. Here, \mathbf{x}_t is the velocity field of the fluid flow at time t . Different types of fluid flows may be classified and labeled according to their degree of turbulence by taking c to be Reynolds number, average vorticity, average magnitude, or a vector of all three. Fluid flows with different Reynolds numbers may have very different dynamics and characteristics.

Formally, let μ be the distribution over $\mathcal{X} \times \mathcal{Y}$ representing the function $f: \mathcal{X} \rightarrow \mathcal{Y}$ where $\mathcal{X} = \mathbb{R}^{d \times l}$ and $\mathcal{Y} = \mathbb{R}^{d \times h}$. Our main assumption is that the domain \mathcal{X} may be partitioned into separate tasks $\mathcal{X} = \cup_{c \in \mathcal{C}} \mathcal{X}_c$ labeled by different task parameter $c \in \mathcal{C}$. Note that the space \mathcal{C} may be either discrete or continuous. Denote the task map $g: \mathcal{X} \rightarrow \mathcal{C}$ taking $x \in \mathcal{X}_c$ to c . Let μ_c be the conditional distribution of $(x, y) \sim \mu$ such that $g(x) = c$.

During training, the model is presented with data from a subset of tasks $\{c_k\} \sim \mathcal{C}$. Our goal is to learn the function $f: \mathcal{X} \rightarrow \mathcal{Y}$ over the whole domain \mathcal{X} which can thus generalize across all tasks $c \in \mathcal{C}$.

2.2. DyAd: Dynamic Adaptation Network

We propose a model-based meta-learning approach for dynamics forecasting. Our approach infers the forecasting task as a latent variable and uses it to adapt the prediction.

Task Inference. Given multiple forecasting tasks, two approaches to modeling f are either to learn all tasks at once or one task at a time. If the training set $S = \{(x^{(i)}, y^{(i)})\}$ has good and uniform coverage of the different classes in \mathcal{X} , that is, if S is a sample from μ i.i.d and is large enough, then a single high capacity neural network may model f well. However, if distribution μ is highly heterogeneous for different c and if the training set is not i.i.d, then a single

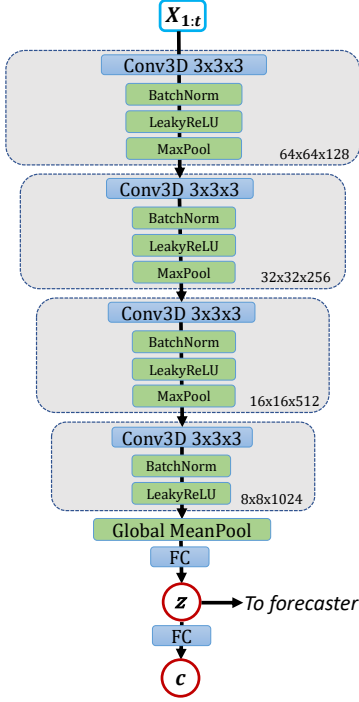


Figure 2. Detail of the DyAd encoder. The conv3D layers are shift equivariant and global mean pooling is shift invariant. The network is approximately invariant to spatial and temporal shifts.

model may struggle with generalization.

We propose to learn the function f in two stages, that is, by first inferring the task c from the input data x and then learning different specialized prediction functions $f_c: \mathcal{X}_c \rightarrow \mathcal{Y}$ for each task $c \in \mathcal{C}$. We introduce a latent variable z_c as a high-dimensional representation for the task c and infer this latent variable from the input data x . As system dynamics are encoded in x , we can use the same single input x to infer the task c and then predict the output label $\hat{y} = f_c(x)$.

Model-Based Adaptation. Care must be taken with how the functions f_c are implemented. A naive approach in which each f_c has its own weights and is trained separately would be highly impractical if the number of tasks $|\mathcal{C}|$ is large. Each f_c would have very little training data and the combined model would have a large number of weights. In essence, treating each c completely separately fails to take advantage of the similarity between tasks f_c .

Our proposal strikes a balance between these two extremes. As shown in Figure 1, our model consists of two parts: an encoder g and prediction network f . The encoder maps the input x to a high-dimensional latent variable z_c that characterizes the dynamics of the system, hence the task c . We then use z_c to adapt the prediction network f to the specific dynamics of the domain c , i.e., model $y = f_c(x)$ as $y = f(x, z_c)$. In this way, we efficiently train different specific mappings f_c for each c . Moreover, the encoder

allows generalization to tasks not in the training set.

Our characteristic latent variable z bears affinity with the “style” vector in style transfer techniques. Rather than aesthetic style in images, our latent variable represents the characteristics of the dynamics that are time-invariant. Interestingly, finding characteristic numbers such as Reynolds number is also a central topic in fluid mechanics. In the style-transfer literature, a generative network is guided by the use of an external style through adaptive instance normalization between convolutional layers (Karras et al., 2019; Huang & Belongie, 2017). We use adaptive instance normalization to incorporate the latent variable z_c into ResNet to create an adaptable prediction network $f_c = f(\cdot, z_c)$.

Partial Disentanglement. The time-invariant characteristic latent variable may be viewed as partial disentanglement of the system state. As suggested by (Locatello et al., 2019; Nie et al., 2020), our disentanglement method is guided by inductive bias and weak supervision. Unlike complete disentanglement, as in e.g. (Massague et al., 2020), in which the latent system state is factored into time-invariant and time-varying components (\bar{z}, \tilde{z}) , our latent variable is only \bar{z} . Nonetheless, \bar{z} provides a strong signal to the prediction network which is useful for generalization.

2.3. Time-shift Invariant Encoder

We assume that c are parameters of the system which are time-invariant, such as constants of motion or fixed parameters of the dynamical system. In order to enforce this inductive bias, we encode time-invariance both in the architecture and training objective of the encoder.

The encoder is implemented using 4 layers of 3D convolution as seen in Figure 2. We convolve across two spatial and one temporal dimension. After this there is a global mean-pooling layer and fully connected layer which outputs the

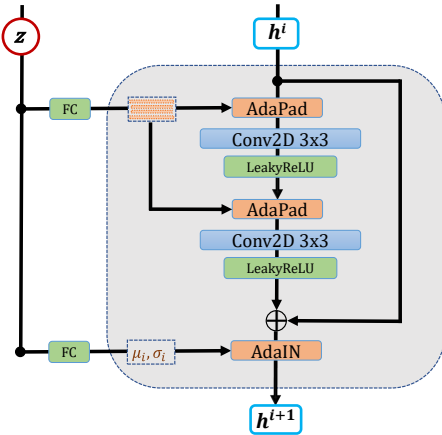


Figure 3. Detail of one block of the prediction network.

estimate of the latent variable \hat{z}_c . One last fully connected layer computes the additional output $\hat{c} = W\hat{z}_c$.

Since convolutions are equivariant to shift (up to boundary frames) and mean pooling is invariant to shift, the encoder is shift-invariant. That is, $\text{enc}(x_1, \dots, x_t, 0) = \text{enc}(0, x_1, \dots, x_t)$. In practice, shifting the time sequence forward one frame will add one new frame at the beginning and drop one frame at the end. This creates some change in output value of the encoder. Thus, practically, the encoder is only approximately shift-invariant.

Following 3D convolutions, we apply BatchNorm, LeakyReLU, and max-pooling. Max-pooling further reduces the theoretical shift-invariance of the network since $2 \times 2 \times 2$ max-pooling is perfectly equivariant to shifts of size 2 and only approximately invariant to shifts of size 1.

2.4. Prediction Network

As shown in Figure 4, our prediction network is similar to ResNet but includes layers which incorporate the characteristic latent variable. We use two specialized layers, adaptive instance normalization AdaIN and adaptive padding AdaPad to specialize the prediction network to specific dynamical systems. AdaIN has been used in style transfer networks to guide generative networks. Here, AdaIN may adapt for specific coefficients and external forces. We also introduce a new layer AdaPad(x, z) which is well-suited for encoding the boundary conditions of dynamical systems.

AdaIN. We employ adaptive instance normalization AdaIN, which has proven effective in the style transfer literature as way to use a style vector to guide a convolutional network (Dumoulin et al., 2016; Ghiasi et al., 2017; Huang & Belongie, 2017; Dumoulin et al., 2018; Karras et al., 2019). Denote the channels of input x by x_i and let $\mu(x_i)$ and $\sigma(x_i)$ be the mean and standard deviation of channel i . For each AdaIN layer, a particular style is computed $s = (\mu_i, \sigma_i)_i = Az + b$, where the linear map A and bias b are learned weights. Adaptive instance normalization is then defined

$$y_i = \sigma_i \frac{x_i - \mu(x_i)}{\sigma(x_i)} + \mu_i.$$

In essence, the channels are renormalized to the style s .

For dynamics prediction, the characteristic latent variable z encodes data analogous to the various coefficients of a differential equation and external forces on the system. In numerical simulation of a differential equation these coefficients enter as scalings of different terms in the equation and the external forces are added to the combined force equation. Thus in our context AdaIN, which scales channels and adds a global vector, is well-suited to injecting this information.

AdaPad. To compliment AdaIN, we introduce the

AdaPad layer, which is specialized to encoding the boundary conditions of each specific dynamical system. Generally when predicting dynamical systems, error is introduced along the boundaries since it is unknown how the dynamics interact with the boundary of the domain, and there may be unknown inflows or outflows. In our method, the boundary conditions may be inferred by the encoder in z and introduced during prediction by AdaPad as padding immediately outside the spatial domain in each layer.

Denote the spatial index of input x by $x_{i,j}$ for $1 \leq i \leq W$ and $1 \leq j \leq H$. Letting A and b be trainable weights, the padding is computed

$$Az + b = (x_{0,0}, \dots, x_{0,H+1}, x_{W+1,0}, \dots, x_{W+1,H+1}, x_{0,1}, \dots, x_{W,0}, x_{W+1,1}, \dots, x_{W,H+1}).$$

Then

$$y = \text{AdaPad}(x, z) = (x_{i,j})_{0 \leq i \leq W+1, 0 \leq j \leq H+1}.$$

Thus y is the input x padded with additional values computed from the latent variable z .

2.5. DyAd Training

We use a two-stage approach for training. The encoder network g_ϕ is trained first separately from the prediction network. To combat the loss of shift invariance from the change from the boundary frames, we train the encoder using a time-shift-invariance loss. Given two training samples $(x^{(i)}, y^{(i)}, c^{(i)})$ and $(x^{(j)}, y^{(j)}, c^{(j)})$ where $x^{(i)}$ and $x^{(j)}$ come from the same task and thus $c^{(i)} = c^{(j)}$, we have loss

$$\mathcal{L}_{\text{enc}} = \mathcal{L}_1(\hat{c}^{(i)}, c^{(i)}) + \alpha \mathcal{L}_2(\hat{z}^{(i)}, \hat{z}^{(j)}) + \beta \|\hat{z}^{(i)}\| - m \quad (3)$$

where estimates $\hat{z}^{(i)} = g_\phi(x^{(i)})$ and $\hat{z}^{(j)} = g_\phi(x^{(j)})$ and $\hat{c}^{(i)} = W\hat{z}^{(i)} + b$ is an affine transformation of z .

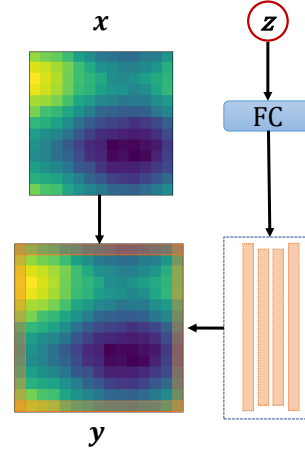


Figure 4. Illustration of the AdaPad operation.

The first term of the loss $\mathcal{L}_1(\hat{c}, c^{(i)})$ allows weak supervision of the latent variable z with input $c^{(i)}$. While not all time-invariant characteristics of the dynamical system are known, domain knowledge of characteristic parameters which identify the dynamics may be incorporated in the datum $c^{(i)}$. For example, the Reynolds number of the fluid.

The second term $\mathcal{L}_2(\hat{z}^{(i)}, \hat{z}^{(j)})$ is the time-shift invariance loss, which penalizes the changes in latent variables between samples. Since the time-shift invariance of convolution is only approximate, this loss term drives the time-shift error even lower. The third term $\|\hat{z}^{(i)}\| - m$ prevents the encoder from generating small $\hat{z}^{(i)}$ due to time-shift invariance loss. For both \mathcal{L}_1 and \mathcal{L}_2 , we use mean squared error.

The prediction network is trained afterwards. The kernels of the convolutions and the fully connected mappings of the AdaIN and AdaPad layers are all trained simultaneously as the prediction network is trained. The loss for the prediction network is the forecasting loss for the true label y ,

$$\mathcal{L}_{\text{pred}} = \mathcal{L}_3(\hat{y}, y).$$

We use MSE per time step and generate multi-step forecasting in an autoregressive fashion.

3. Theoretical Analysis

The high-level idea of our method is to learn a good representation of the dynamics that generalizes well and adapt this representation to new tasks. Our model achieves this by learning on a heterogeneous domain where it learns to infer the tasks. We provide analysis for this procedure. See Appendix B for a longer treatment with proofs.

Suppose we have K tasks, each of which is sampled from a continuous space $\{c_k\}_{k=1}^K \sim \mathcal{C}$. For each task c_k , we have a collection of series as realizations from the dynamical system $\mathcal{X}_k = \{(\mathbf{x}_t, \dots, \mathbf{x}_1; c_k)^{(i)}\}_{i=1}^{n_k}$ where c_k represents the system behavior in a specific domain. Let $\mathcal{X} = \cup_{c \in \mathcal{C}} \mathcal{X}_c$ be the union of samples over all tasks.

Multi-task Learning Error. Our model resembles the multi-task representation learning setting (Maurer et al., 2016) with joint risk $\epsilon = (1/K) \sum_k \epsilon_k$ the mean of risks ϵ_k of each task defined separately. Denote the corresponding empirical risks $\hat{\epsilon}$ and $\hat{\epsilon}_k$. We bound the true risk ϵ using the empirical risk $\hat{\epsilon}$ and Rademacher complexity $R(\mathcal{F})$ of the hypothesis class \mathcal{F} . The following theorem restates the main result in (Ando et al., 2005) with simplified notations.

Theorem 3.1. (Ando et al., 2005) *Assume loss is bounded $l \leq 1/2$. Given n samples each from K different forecasting tasks μ_1, \dots, μ_k with probability at least $1 - \delta$, the following inequality holds for each $f \in \mathcal{F}$:*

$$\frac{1}{K} \sum_k \epsilon_k(f) \leq \frac{1}{K} \sum_k \hat{\epsilon}_k(f) + 2R(\mathcal{F}) + \sqrt{\frac{\log 1/\delta}{2nK}}$$

The following inequality compares the performance for multi-task learning to learning the individual tasks. Let $R_k(\mathcal{F})$ be the Rademacher complexity for \mathcal{F} over μ_k .

Lemma 3.2. *The Rademacher complexity for multi-task learning is bounded $R(\mathcal{F}) \leq (1/K) \sum_{k=1}^K R_k(\mathcal{F})$.*

We can now compare the bound from Theorem 3.1 with the bound obtained by considering each task individually.

Proposition 3.3. *Assume the loss is bounded $l \leq 1/2$, then the generalization bound given by considering each task individually is*

$$\epsilon(f) \leq \hat{\epsilon}(f) + 2 \left(\frac{1}{K} \sum_{k=1}^K R_k(\mathcal{F}) \right) + \sqrt{\frac{\log 1/\delta}{2n}}. \quad (4)$$

which is strictly looser than the bound from Theorem 3.1.

This helps explain why our multitask learning framework has better generalization than learning each task independently. The shared data tightens the generalization bound.

Domain Adaptation Error. Since we test on $c \sim \mathcal{C}$ outside the training set $\{c_k\}$, we incur error due to domain adaptation from the source domains $\mu_{c_1}, \dots, \mu_{c_K}$ to target domain μ_c with μ being the true distribution. Denote the corresponding empirical distributions of n samples per task by $\hat{\mu}_c$. For similar domains, the Wasserstein distance $W_1(\mu_c, \mu_{c'})$ is small. The bound from (Redko et al., 2017) applies well to our setting as such:

Theorem 3.4 ((Redko et al., 2017), Theorem 2). *Let $\lambda = \min_{f \in \mathcal{F}} (\epsilon_c(f) + 1/K \sum_{k=1}^K \epsilon_{c_k}(f))$. There is $N = N(\zeta, \dim(\mathcal{X}))$ such that for $n > N$, for any hypothesis f , with probability at least $1 - \delta$,*

$$\begin{aligned} \epsilon_c(f) &\leq \frac{1}{K} \sum_{k=1}^K \epsilon_{c_k}(f) + W_1 \left(\hat{\mu}_c, \frac{1}{K} \sum_{k=1}^K \hat{\mu}_{c_k} \right) \\ &\quad + \sqrt{2 \log(1/\delta)} \left(\sqrt{1/n} + \sqrt{1/(nK)} \right) + \lambda. \end{aligned}$$

Encoder versus Prediction Network Error. Error from DyAd may result from either the encoder g_ϕ or the prediction network f_θ . Our hypothesis space has the form $\{x \mapsto f_\theta(x, g_\phi(x))\}$ where ϕ and θ are the weights of the encoder and prediction network respectively. Let $\epsilon_{\mathcal{X}}$ be the error over the entire domain \mathcal{X} , that is, for all c . Let $\epsilon_{\text{enc}}(g_\phi) = \mathbb{E}_{x \sim \mathcal{X}} (\mathcal{L}_1(g(x), g_\phi(x)))$ be the encoder error.

Proposition 3.5. *Assume $c \mapsto \sup_\theta (f_\theta(\cdot, c))$ is Lipschitz continuous with Lipschitz constant γ . Then we bound*

$$\epsilon_{\mathcal{X}}(f_\theta(\cdot, g_\phi(\cdot))) \leq \gamma \epsilon_{\text{enc}}(g_\phi) + \mathbb{E}_{c \sim \mathcal{C}} [\epsilon_c(f_\theta(x, c))] \quad (5)$$

where the first term is the error due to the encoder incorrectly identifying the task and the second term is the error due to the prediction network alone.

4. Related Work

Learning Dynamical Systems. Deep learning models are gaining popularity for learning dynamical systems (Shi et al., 2017; Chen et al., 2018; Kolter & Manek, 2019; Azencot et al., 2020a). An emerging topic is physics-informed deep learning Raissi et al. (2017); Maziar Raissi (2019); Lutter et al. (2018); Azencot et al. (2020b); Wang et al. (2020a) which integrates inductive biases from physical systems to improve learning. For example, (Maziar Raissi, 2019) use deep neural networks to solve PDEs automatically but require explicit input of boundary conditions during inference. (Lutter et al., 2018) encode Euler-Lagrange equation into the deep neural nets but focus on learning low-dimensional trajectories. For high-dimensional fluid flow, (Xie et al., 2018) and (Tompson et al., 2017) developed deep learning models in the context of fluid flow animation, where the prediction and physical consistency is less critical. There are also physics-informed deep learning models (de Bezenac et al., 2018; Wang et al., 2020b; Ayed et al., 2019a;b; Li et al., 2021). For instance, Anderson et al. (2019) designed rotationally covariant neural network for learning molecular systems. Morton et al. (2018); Azencot et al. (2020b) incorporated Koopman theory into the architecture. However, these approaches often focus on a specific type of system dynamics instead of meta-learning in this work.

Meta-learning and Domain Adaptation. The aim of meta learning, or learning to learn (Thrun & Pratt, 1998), is to acquire generic knowledge of different tasks in order for rapid learning on new tasks. Based on how the meta-level knowledge is extracted and used, meta-learning methods have been classified into model-based (Munkhdalai & Yu, 2017; Duan et al., 2017; Santoro et al., 2016; Alet et al., 2018; Oreshkin et al., 2019; Seo et al., 2020), metric-based (Vinyals et al., 2016; Snell et al., 2017) and gradient-based (Finn et al., 2017; Andrychowicz et al., 2016; Rusu et al., 2019; Grant et al., 2018; Yao et al., 2019). Most meta-learning approaches are outside of the forecasting domain with a few exceptions. Oreshkin et al. (2019) design a residual architecture for time series forecasting with a meta-learning parallel. Alet et al. (2018) propose a modular meta-learning approach to combine neural network modules for continues control. But forecasting physical dynamics poses unique challenges to meta-learning as we seek ways to encode physical knowledge into our model. DyAd can also be considered as a meta-learning model since the encoder is able to encode different tasks and extract high-level meta representations and the forecaster then performs across different systems without retraining. It is noteworthy that meta-learning for time series forecasting (Lemke & Gabrys, 2010; Talagala et al., 2018) was termed for forecast model selection, which has a different objective from ours.

Style Transfer. Our approach is inspired by the style

transfer techniques. Style transfer initially appear in non-photorealistic rendering (Kyprianidis et al., 2012). Recently, neural style transfer (Jing et al., 2019) has been applied to image synthesis (Gatys et al., 2016), videos generation (Ruder et al., 2016), and language translation (Prabhumoye et al., 2018). For dynamical systems, Sato et al. (2018) adapts texture synthesis to transfer the style of turbulence for animation. Kim & Lee (2019) studies unsupervised generative modeling of turbulent flows but for super-resolution reconstruction rather than forecasting.

5. Experiments

We compare our model with a series of baselines on the multi-step forecasting with different dynamics. We consider two testing scenarios: (1) dynamics with different initial conditions (test-future) and (2) dynamics with different parameters such as external force (test-domain). The first scenario evaluates the models’ ability to extrapolate into the future for the same task. The second scenario estimates the capability of the models to generalize across different tasks.

We experiment on synthetic turbulent flows, real-world sea surface temperature and ocean currents data. They are difficult to forecast using numerical methods due to unknown external forces and complex dynamics not fully captured by simplified mathematical models. We defer the details of the datasets and experiments to Appendix A.2.

5.1. Datasets

Turbulent Flow with Varying Buoyancy. We generate a synthetic dataset of turbulent flows with a numerical simulator, PhiFlow¹. It contains 64×64 velocity fields of turbulent flows in which we vary the buoyant force acting on the fluid from 1 to 25. Each buoyant force corresponds to a forecasting task and there are 25 tasks in total. We use the mean vorticity of each task as partial supervision c as we can directly calculate it from the data. Vorticity can characterize formation and circular motion of turbulent flows.

Sea Surface Temperature. We evaluate on a real-world sea surface temperature data generated by the NEMO ocean engine (Madec et al., 2015)². We select an area from Pacific ocean range from 01/01/2018 to 12/31/2020. The corresponding latitude and longitude are (-174~153, 5~26). This area is then divided into 25 64×64 subregions, each is a task since the mean temperature varies a lot along longitude and latitude. For the encoder training, we use season as an additional supervision signal besides the mean temperature of each subregion. In other words, the encoder should

¹<https://github.com/tum-pbs/PhiFlow>

²The data are available at https://resources.marine.copernicus.eu/?option=com_csw&view=details&product_id=GLOBAL_ANALYSIS_FORECAST_PHY_001_024

Table 1. Prediction RMSE on the turbulent flow and sea surface temperature datasets. Prediction RMSE and ESE (energy spectrum errors) on the test-future and test-domain test sets of ocean currents dataset.

Model	Turbulent Flows		Sea Temperature		Ocean Currents	
	test-future	test-domain	test-future	test-domain	test-future	test-domain
ResNet	0.936 \pm 0.098	0.652 \pm 0.019	1.522 \pm 0.099	1.504 \pm 0.078	1.172 \pm 0.091 0.942 \pm 0.139	1.148 \pm 0.036 1.136 \pm 0.117
U-Net	0.921 \pm 0.020	0.675 \pm 0.021	1.106 \pm 0.142	1.137 \pm 0.153	1.116 \pm 0.103 0.756 \pm 0.056	1.154 \pm 0.118 0.876 \pm 0.083
Mod-ind	1.126 \pm 0.050	—	2.486 \pm 0.167	—	1.305 \pm 0.156 1.160 \pm 0.096	— —
Mod-attn	0.626 \pm 0.022	0.919 \pm 0.026	2.039 \pm 0.139	2.038 \pm 0.118	1.200 \pm 0.177 0.804 \pm 0.121	1.224 \pm 0.119 1.109 \pm 0.084
Mod-wt	0.579 \pm 0.033	0.601 \pm 0.071	0.834 \pm 0.093	0.721 \pm 0.101	1.220 \pm 0.092 0.835 \pm 0.044	1.245 \pm 0.108 1.300 \pm 0.073
MetaNet	0.759 \pm 0.132	0.764 \pm 0.079	2.911 \pm 0.219	1.938 \pm 0.171	1.245 \pm 0.086 0.971 \pm 0.097	1.240 \pm 0.087 1.269 \pm 0.040
MAML	0.627 \pm 0.003	0.677 \pm 0.019	1.862 \pm 0.187	1.935 \pm 0.039	1.387 \pm 0.191 1.077 \pm 0.124	1.297 \pm 0.143 1.199 \pm 0.086
DyAd	0.423\pm0.011	0.533\pm0.017	0.741\pm0.063	0.689\pm0.062	1.006\pm0.067 0.486\pm0.041	0.955\pm0.093 0.544\pm0.113

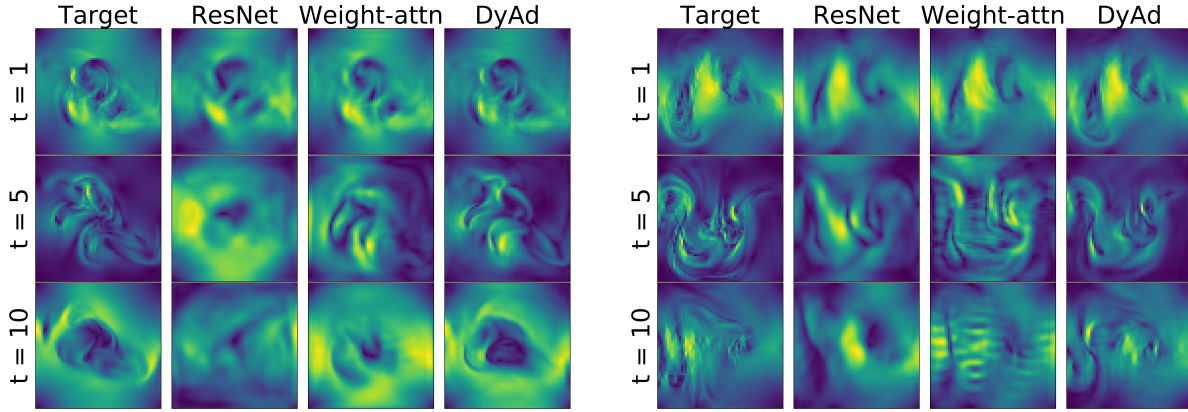


Figure 5. Target and predictions by ResNet, Modular-wt and DyAd at time 1, 5, 10 for turbulent flows with buoyancy factors 9 (left) and 21 (right) respectively. We can see that DyAd can easily generate predictions for various flows while ResNet and Modular-wt have trouble understanding and disentangling buoyancy factors.

be able to infer the mean temperature of the subregion as well as to classify four seasons given the temperature series.

Ocean Currents. We also experiment with the velocity fields of ocean currents from the same region and use the same task division as the sea surface temperature data set. Similar to the turbulent flow data set, we use the mean vorticity of each subregion as the weak-supervision signal.

5.2. Baselines

We include several SoTA baselines from meta-learning, as well as common methods for dynamics forecasting.

- ResNet (He et al., 2016): A widely adopted video prediction model (Oprea et al., 2020; Wang et al., 2020b).
- U-net (Ronneberger et al., 2015): Originally developed for biomedical image segmentation, adapted for dynamics forecasting (de Bezenac et al., 2018)
- Mod-ind: A simple baseline with independent neural network modules trained for different tasks.
- Mod-attn: A modular meta-learning method which combines modules to generalize to new tasks (Alet et al., 2018). Attention mechanism is used to combine

modules through the final output.

- Mod-wt: A modular meta-learning variant which uses attention weights to combine the parameters of the convolutional kernels for new tasks.
- MetaNet (Munkhdalai & Yu, 2017): A model-based meta-learning method which requires a few labels from test tasks as a support set to adapt.
- MAML (Finn et al., 2017): A popular gradient-based meta-learning approach. We replaced the classifier in the original model with a ResNet for regression.

Both Mod-attn and Mod-wt have a convolutional encoder to generate attention weights. MetaNet requires a few samples from test tasks as a support set and MAML needs adaptation retraining on test tasks, while other models do not need any information from the test domains. Details about baselines can be found in Appendix A.2.

5.3. Experiment Setup

For all datasets, we use a sliding window approach to generate samples of sequences. For test-future, we train and test on the same tasks but different time steps. For test-domain, we train and test on different tasks with a 80-20 split. All

models are trained to make next step prediction given the previous 20 steps as input. We forecast in an autoregressive manner to generate multi-step ahead predictions. All results are averaged over 3 runs with random initialization.

Apart from root mean square error, we also report the energy spectrum error for ocean current prediction which is the RMSE regarding the log of energy spectrum. ESE can indicate whether the predictions preserve the correct statistical distribution and obey the energy conservation law, which is a critical metric for physical consistency. Details about energy spectrum can be found in Appendix A.3.

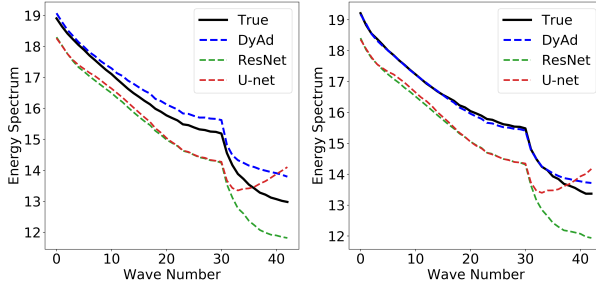


Figure 6. The energy spectrum of target and predictions by ResNet, U-net and DyAd on future test set (left) and domain test set (right) of ocean currents.

5.4. Experiment Results

Prediction Performance. Table 1 shows the RMSE of 10-step ahead predictions on two test sets of turbulent flows and sea surface temperature, and DyAd makes the most accurate predictions for both test sets of both datasets. Figure 5 shows the target and predictions by ResNet, Modular-wt and DyAd at time 1, 5, 10 for turbulent flows with buoyancy factors 9 (left) and 21 (right) respectively. We can see that DyAd can generate realistic flows with the corresponding characteristics while the other two models have trouble understanding and disentangling the buoyancy factor.

Table 1 also reports the RMSE and ESE of 20-step ahead ocean currents predictions. DyAd not only has small RMSE but also obtains the smallest ESE, suggesting it captures the statistical distribution of ocean currents well. Figure 6 shows the energy spectrum of target and predictions by ResNet, U-net and DyAd on two test sets of ocean currents, and we can see that DyAd is the closest to the target.

Ablation Study. We also performed an ablation study of DyAd to understand the contribution of each component, shown in Table 2. We first remove the encoder from DyAd while keeping the same prediction network (No_enc). The resulting model degrades but still outperforms ResNet. This demonstrates the effectiveness of AdaIN and AdaPad for prediction. Another notable feature of our model is the ability to infer tasks with weakly supervised signal c . It is

Table 2. Ablation study: prediction RMSE of DyAd, DyAd without encoder, DyAd with encoder trained by wrong supervision c and DyAd with end to end training.

Model	test-future	test-domain
DyAd(ours)	0.423 \pm 0.011	0.533 \pm 0.017
No_enc	0.627 \pm 0.033	0.601 \pm 0.022
Wrong_enc	0.658 \pm 0.019	0.617 \pm 0.031
End2End	0.449 \pm 0.003	0.536 \pm 0.003

important to have a c that is related to the task domain. As an ablative study, we fed the encoder in DyAd a random c , leading to Wrong_enc. We see that having the wrong supervision may hurt the forecasting performance. We also tried to train DyAd end-to-end (End2End) but observed worse performance than the two-stage training approach.

Controllable Forecast. DyAd infers the characteristic latent variable from data, which allows direct control of the latent characteristics. We tried to vary the encoder input while keeping the prediction network input fixed. Figure 7 shows the outputs from DyAd when the encoder is fed with flow with different buoyancy factors $c = 5, 15, 25$. We can see with higher buoyancy factors, the predictions become more turbulent. This demonstrates that the encoder can disentangle and control the latent characteristics of predictions.

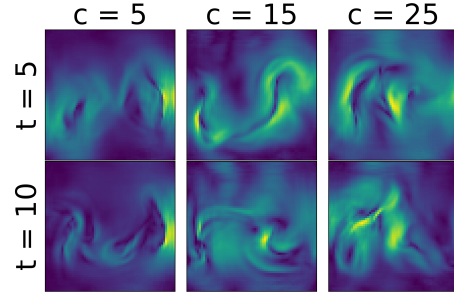


Figure 7. Outputs from DyAd while we vary encoder input but keep the prediction network input fixed. From left to right, the encoder is fed with flow with different buoyancy factor $c = 5, 15, 25$. The prediction network input has fixed buoyancy $c = 15$.

6. Conclusion

We propose a model-based meta-learning method, DyAd to forecast physical dynamics. DyAd uses an encoder to infer the parameters of the task and a prediction network to adapt and forecast giving the inferred task. Our model can also leverage any weak supervision signals that can help distinguish different tasks, allowing the incorporation of additional domain knowledge. On challenging turbulent flow prediction and real-world ocean temperature and currents forecasting tasks, we observe superior performance of our model across heterogeneous dynamics. Future work would consider non-grid data such as flows on a graph or a sphere.

References

Alet, F., Lozano-Perez, T., and Kaelbling, L. Modular meta-learning. *ArXiv*, abs/1806.10166, 2018.

Anderson, B., Hy, T.-S., and Kondor, R. Cormorant: Covariant molecular neural networks. In *Advances in neural information processing systems (NeurIPS)*, 2019.

Ando, R. K., Zhang, T., and Bartlett, P. A framework for learning predictive structures from multiple tasks and unlabeled data. *Journal of Machine Learning Research*, 6(11), 2005.

Andrychowicz, M., Denil, M., Colmenarejo, S. G., Hoffman, M. W., Pfau, D., Schaul, T., and Freitas, N. D. Learning to learn by gradient descent by gradient descent. In *Advances in Neural Information Processing Systems*, 2016.

Ayed, I., Bézenac, E. D., Pajot, A., and Gallinari, P. Learning partially observed PDE dynamics with neural networks, 2019a. URL <https://openreview.net/forum?id=HyefgnCqFm>.

Ayed, I., de Bézenac, E., Pajot, A., Brajard, J., and Gallinari, P. Learning dynamical systems from partial observations. *ArXiv*, abs/1902.11136, 2019b.

Azencot, O., Erichson, N., Lin, V., and Mahoney, M. W. Forecasting sequential data using consistent koopman autoencoders. In *International Conference on Machine Learning*, 2020a.

Azencot, O., Erichson, N. B., Lin, V., and Mahoney, M. Forecasting sequential data using consistent koopman autoencoders. In *International Conference on Machine Learning*, pp. 475–485. PMLR, 2020b.

Baxter, J. Theoretical models of learning to learn. In *Learning to learn*, pp. 71–94. Springer, 1998.

Chen, R. T., Rubanova, Y., Bettencourt, J., and Duvenaud, D. Neural ordinary differential equations. In *Proceedings of the 32nd International Conference on Neural Information Processing Systems*, pp. 6572–6583, 2018.

de Bezenac, E., Pajot, A., and Gallinari, P. Deep learning for physical processes: Incorporating prior scientific knowledge. In *International Conference on Learning Representations*, 2018. URL <https://openreview.net/forum?id=By4HsfWAZ>.

Duan, Y., Andrychowicz, M., Stadie, B. C., Ho, J., Schneider, J., Sutskever, I., Abbeel, P., and Zaremba, W. One-shot imitation learning. In *Advances in Neural Information Processing Systems*, 2017.

Dumoulin, V., Shlens, J., and Kudlur, M. A learned representation for artistic style. *arXiv preprint arXiv:1610.07629*, 2016.

Dumoulin, V., Perez, E., Schucher, N., Strub, F., Vries, H. d., Courville, A., and Bengio, Y. Feature-wise transformations. *Distill*, 3(7):e11, 2018.

Finn, C., Abbeel, P., and Levine, S. Model-agnostic meta-learning for fast adaptation of deep networks. In *International Conference on Machine Learning*, 2017.

Gatys, L. A., Ecker, A. S., and Bethge, M. Image style transfer using convolutional neural networks. In *Proceedings of the IEEE conference on computer vision and pattern recognition*, pp. 2414–2423, 2016.

Ghiasi, G., Lee, H., Kudlur, M., Dumoulin, V., and Shlens, J. Exploring the structure of a real-time, arbitrary neural artistic stylization network. *arXiv preprint arXiv:1705.06830*, 2017.

Grant, E., Finn, C., Levine, S., Darrell, T., and Griffiths, T. Recasting gradient-based meta-learning as hierarchical bayes. *ArXiv Preprint*, abs/1801.08930, 2018.

Gupta, A., Mendonca, R., Liu, Y., Abbeel, P., and Levine, S. Meta-reinforcement learning of structured exploration strategies. In *Proceedings of the 32nd International Conference on Neural Information Processing Systems*, pp. 5307–5316, 2018.

He, K., Zhang, X., Ren, S., and Sun, J. Deep residual learning for image recognition. In *Proceedings of the IEEE conference on computer vision and pattern recognition*, pp. 770–778, 2016.

Huang, X. and Belongie, S. Arbitrary style transfer in real-time with adaptive instance normalization. In *Proceedings of the IEEE International Conference on Computer Vision*, pp. 1501–1510, 2017.

Jing, Y., Yang, Y., Feng, Z., Ye, J., Yu, Y., and Song, M. Neural style transfer: A review. *IEEE transactions on visualization and computer graphics*, 26(11):3365–3385, 2019.

Karras, T., Laine, S., and Aila, T. A style-based generator architecture for generative adversarial networks. In *Proceedings of the IEEE/CVF Conference on Computer Vision and Pattern Recognition*, pp. 4401–4410, 2019.

Kim, J. and Lee, C. Deep unsupervised learning of turbulence for inflow generation at various reynolds numbers. *arXiv:1908.10515*, 2019.

Kolter, J. Z. and Manek, G. Learning stable deep dynamics models. In *Advances in Neural Information Processing Systems (NeurIPS)*, volume 32, pp. 11128–11136, 2019.

Kyprianidis, J. E., Collomosse, J., Wang, T., and Isenberg, T. State of the "art": A taxonomy of artistic stylization techniques for images and video. *IEEE transactions on visualization and computer graphics*, 19(5):866–885, 2012.

Lemke, C. and Gabrys, B. Meta-learning for time series forecasting and forecast combination. *Neurocomputing*, 73(10-12):2006–2016, 2010.

Li, Z., Kovachki, N., Azizzadenesheli, K., Liu, B., Bhattacharya, K., Stuart, A., and Anandkumar, A. Fourier neural operator for parametric partial differential equations. *International Conference on Learning Representations*, 2021.

Locatello, F., Bauer, S., Lucic, M., Raetsch, G., Gelly, S., Schölkopf, B., and Bachem, O. Challenging common assumptions in the unsupervised learning of disentangled representations. In *international conference on machine learning*, pp. 4114–4124. PMLR, 2019.

Lutter, M., Ritter, C., and Peters, J. Deep lagrangian networks: Using physics as model prior for deep learning. In *International Conference on Learning Representations*, 2018.

Madec, G. et al. NEMO ocean engine, 2015. Technical Note. Institut Pierre-Simon Laplace (IPSL), France. https://epic.awi.de/id/eprint/39698/1/NEMO_book_v6039.pdf.

Massague, A. C., Zhang, C., Feric, Z., Camps, O., and Yu, R. Learning disentangled representations of video with missing data. *arXiv preprint arXiv:2006.13391*, 2020.

Maurer, A., Pontil, M., and Romera-Paredes, B. The benefit of multitask representation learning. *Journal of Machine Learning Research*, 17(81):1–32, 2016.

Maziar Raissi, Paris Perdikaris, G. E. K. Physics-informed neural networks: A deep learning framework for solving forward and inverse problems involving nonlinear partial differential equations. *Journal of Computational Physics*, 378:686–707, 2019.

Mohri, M., Rostamizadeh, A., and Talwalkar, A. *Foundations of machine learning*. MIT press, 2018.

Morton, J., Jameson, A., J. Kochenderfer, M., and Witherden, F. Deep dynamical modeling and control of unsteady fluid flows. In *Advances in Neural Information Processing Systems (NeurIPS)*, 2018.

Munkhdalai, T. and Yu, H. Meta networks. *Proceedings of machine learning research*, 70:2554–2563, 2017.

Nie, W., Karras, T., Garg, A., Debhath, S., Patney, A., Patel, A. B., and Anandkumar, A. Semi-supervised stylegan for disentanglement learning. In *International Conference on Machine Learning*, 2020.

Oprea, S., Martinez-Gonzalez, P., Garcia-Garcia, A., Castro-Vargas, J. A., Orts-Escalano, S., Garcia-Rodriguez, J., and Argyros, A. A review on deep learning techniques for video prediction. *IEEE Transactions on Pattern Analysis and Machine Intelligence*, 2020.

Oreshkin, B. N., Carpow, D., Chapados, N., and Bengio, Y. N-beats: Neural basis expansion analysis for interpretable time series forecasting. In *International Conference on Learning Representations*, 2019.

Prabhumoye, S., Tsvetkov, Y., Salakhutdinov, R., and Black, A. W. Style transfer through back-translation. In *Proceedings of the 56th Annual Meeting of the Association for Computational Linguistics (Volume 1: Long Papers)*, pp. 866–876, 2018.

Raissi, M., Perdikaris, P., and Karniadakis, G. E. Physics informed deep learning (part i): Data-driven solutions of nonlinear partial differential equations. *arXiv preprint arXiv:1711.10561*, 2017.

Redko, I., Habrard, A., and Sebban, M. Theoretical analysis of domain adaptation with optimal transport. In *Joint European Conference on Machine Learning and Knowledge Discovery in Databases*, pp. 737–753. Springer, 2017.

Ronneberger, O., Fischer, P., and Brox, T. U-net: Convolutional networks for biomedical image segmentation. In *International Conference on Medical image computing and computer-assisted intervention*, pp. 234–241. Springer, 2015.

Ruder, M., Dosovitskiy, A., and Brox, T. Artistic style transfer for videos. In *German conference on pattern recognition*, pp. 26–36. Springer, 2016.

Rusu, A. A., Rao, D., Sygnowski, J., Vinyals, O., Pascanu, R., Osindero, S., and Hadsell, R. Meta-learning with latent embedding optimization. In *International Conference on Learning Representations*, 2019. URL <https://openreview.net/forum?id=BJgk1hAcK7>.

Santoro, A., Bartunov, S., Botvinick, M., Wierstra, D., and Lillicrap, T. Meta-learning with memory-augmented neural networks. In *ICML*, 2016.

Sato, S., Dobashi, Y., Kim, T., and Nishita, T. Example-based turbulence style transfer. *ACM Transactions on Graphics (TOG)*, 37(4):1–9, 2018.

Seo, S., Meng, C., Rambhatla, S., and Liu, Y. Physics-aware spatiotemporal modules with auxiliary tasks for meta-learning. *ArXiv*, abs/2006.08831, 2020.

Shi, X., Gao, Z., Lausen, L., Wang, H., Yeung, D., Wong, W., and chun Woo, W. Deep learning for precipitation nowcasting: A benchmark and a new model. In *Advances in neural information processing systems*, 2017.

Snell, J., Swersky, K., and Zemel, R. Prototypical networks for few-shot learning. In *Advances in Neural Information Processing Systems*, 2017.

Talagala, T. S., Hyndman, R. J., Athanasopoulos, G., et al. Meta-learning how to forecast time series. Technical report, Monash University, Department of Econometrics and Business Statistics, 2018.

Thrun, S. and Pratt, L. Learning to learn: Introduction and overview. In *Learning to learn*, pp. 3–17. Springer, 1998.

Tompson, J., Schlachter, K., Sprechmann, P., and Perlin, K. Accelerating Eulerian fluid simulation with convolutional networks. In *ICML’17 Proceedings of the 34th International Conference on Machine Learning*, volume 70, pp. 3424–3433, 2017.

Vinyals, O., Blundell, C., Lillicrap, T., Kavukcuoglu, K., and Wierstra, D. Matching networks for one shot learning. In *NIPS*, 2016.

Wang, R., Kashinath, K., Mustafa, M., Albert, A., and Yu, R. Towards physics-informed deep learning for turbulent flow prediction. In *Proceedings of the 26th ACM SIGKDD International Conference on Knowledge Discovery & Data Mining*, pp. 1457–1466, 2020a.

Wang, R., Walters, R., and Yu, R. Incorporating symmetry into deep dynamics models for improved generalization. *arXiv preprint arXiv:2002.03061*, 2020b.

Xie, Y., Franz, E., Chu, M., and Thuerey, N. tempoGAN: A temporally coherent, volumetric GAN for super-resolution fluid flow. *ACM Transactions on Graphics (TOG)*, 37(4):95, 2018.

Yao, H., Wei, Y., Huang, J., and Li, Z. Hierarchically structured meta-learning. In *International Conference on Machine Learning*, pp. 7045–7054. PMLR, 2019.

Yoon, J., Kim, T., Dia, O., Kim, S., Bengio, Y., and Ahn, S. Bayesian model-agnostic meta-learning. In *Proceedings of the 32nd International Conference on Neural Information Processing Systems*, pp. 7343–7353, 2018.

Zoltowski, D., Pillow, J., and Linderman, S. A general recurrent state space framework for modeling neural dynamics during decision-making. In *International Conference on Machine Learning*, pp. 11680–11691. PMLR, 2020.

A. Implementation Details

A.1. Model Design

The prediction network $\hat{y} = f(x, z)$ is composed of 8 blocks. Each block operates on a hidden state $h^{(i)}$ of shape $B \times H \times W \times C_{\text{in}}$ and yields a new hidden state $h^{(i+1)}$ of the shape $B \times H \times W \times C_{\text{out}}$. The first input is $h_0 = x$ and the final output is computed from the final hidden state as $\hat{y} = \text{Conv2D}(h^{(8)})$. We define each block as

$$\begin{aligned} a^{(i)} &= \sigma(\text{Conv2D}(\text{AdaPad}(h^{(i)}, z))) \\ b^{(i)} &= \sigma(\text{Conv2D}(\text{AdaPad}(a^{(i)}, z))) + h^{(i)} \\ h_{i+1} &= \text{AdaIN}(b^{(i)}, z) \end{aligned}$$

as illustrated in Figure 4.

A.2. Experiment Details

For fair comparison, we set these models to have equal capacity as DyAd in terms of number of parameters. Hyperparameters including learning rate, input length and the number of steps of accumulated loss for training are tuned on validation sets.

Baselines. Modular-attn has a convolutional encoder f that takes the same input x as each module M to generate attention weights, $\sum_{l=1}^m \frac{\exp[f(x)(l)]}{\sum_{k=1}^m \exp[f(x)(k)]} M_l(x)$. Modular-wt also has the same encoder but to generate weights for combining the convolution parameters of all modules. We use additional samples of up to 20% of the test set from test tasks. MetaNet uses these as a support set. MAML is retrained on these samples for 10 epoch for adaptation.

Hyperparameter tuning. We tuned learning rate (1e-3~1e-5), batch size (16~64), the number of accumulated errors for backpropagation (2~5), and hidden size (64~512) of Modular Networks and Meta-Nets. We fixed the number of historic input frames as 20. When we trained the encoder on turbulent flows and sea surface temperature, we used $\alpha = 1$ and $\beta = 1$. For ocean currents, we used $\alpha = 0.2$ and $\beta = 0.2$.

Model Capacity. Table 3 displays the number of parameters of each tuned model.

ResNet	U-net	Mod-ind	Mod-attn	Mod-wt	MetaNets	MAML	DyAd
20.32	9.69	13.01	13.19	13.19	9.63	20.32	15.60

Table 3. The number of parameters of each model.

A.3. Turbulence kinetic energy spectrum

The turbulence kinetic energy spectrum $E(k)$ is related to the mean turbulence kinetic energy as

$$\begin{aligned} \int_0^\infty E(k) dk &= (\overline{(u')^2} + \overline{(v')^2})/2, \\ \overline{(u')^2} &= \frac{1}{T} \sum_{t=0}^T (u(t) - \bar{u})^2, \end{aligned}$$

where the k is the wavenumber and t is the time step. Figure 8 shows a theoretical turbulence kinetic energy spectrum plot. The spectrum can describe the transfer of energy from large scales of motion to the small scales and provides a representation of the dependence of energy on frequency. Thus, the Energy Spectrum Error can indicate whether the predictions preserve the correct statistical distribution and obey the energy conservation law. A trivial example that can illustrate why we need ESE is that if a model simply outputs moving averages of input frames, the accumulated RMSE of predictions might not be high but the ESE would be really big because all the small or even medium eddies are smoothed out.

B. Theoretical Analysis

The high-level idea of our method is to learn a good representation of the underlying dynamics from multiple tasks, and then transfer this representation to a target task (domain adaptation).

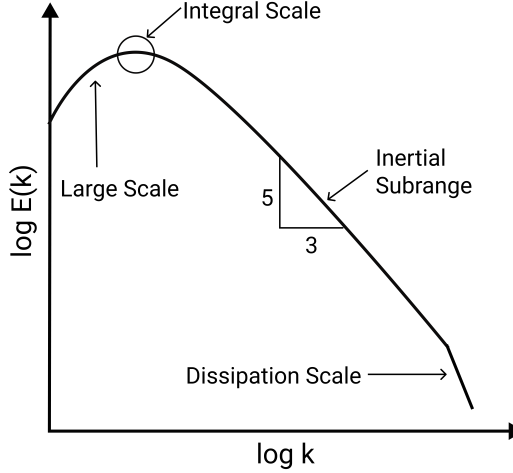


Figure 8. Spectrum plot

Definition 1 (Forecasting task). *Each forecasting task $\mathbf{x}_{t+1} = f(\mathbf{x}_t, \dots)$ is to learn a conditional distribution μ over the system states $\mu : p(\mathbf{x}_{t+1} | \mathbf{x}_t, \dots)$ conditioned on the sequence of previous states where μ is a probability measure.*

In our setting, we have K tasks, each of which is sampled from a continuous, finite space $\{c_k\} \sim \mathcal{C}$. Let μ_k be the corresponding conditional probability measure $p(\mathbf{x}_t, \dots, \mathbf{x}_1 | c_k)$. For each task c_k , we have a collection of n series as realizations from the dynamical system $\mathbf{X}_k = \{(\mathbf{x}_t, \dots, \mathbf{x}_1; c_k)^{(i)}\}_{i=1}^n$ sampled from μ_k . The semicolon here represents the system behavior in a specific domain c_k . Let $\mathbf{X} = \bigcup_k \mathbf{X}_k$ be the union of samples over all tasks.

In practice, we often have some intuition of the variables that dictate the domain. Therefore, we have two possible scenarios for the role of c in dynamical systems:

1. c fully distinguishes the task: the differences in \mathbf{X}_k can be completely explained by the differences in c_k ;
2. c partially distinguishes the task: a more realistic scenario where we only have partial knowledge of the domain. There exist latent variables z' that need to be inferred from raw data. Together $z = [c, z']$ can describe the behavior of the system in a domain.

We assume Scenario 1, which resembles the multi-task representation learning setting (Maurer et al., 2016) with joint true risk over all tasks ϵ and individual task true risk ϵ_k defined respectively

$$\epsilon(f) = \frac{1}{K} \sum_{k=1}^K \epsilon_k(f), \quad \epsilon_k(f) = \mathbb{E}_{\mathbf{x}_k^{(i)} \sim \mu_k} [l(f(\mathbf{x}_k^{(i)}))] \quad (6)$$

and corresponding empirical risks

$$\hat{\epsilon}(f, \mathbf{X}) = \frac{1}{K} \sum_{k=1}^K l(f(\mathbf{X}_k)), \quad \hat{\epsilon}_k(f, \mathbf{X}_k) = l(f(\mathbf{X}_k)),$$

where l is a loss function.

B.1. Multi-Task Learning Error

We want to bound the true loss ϵ using the empirical loss $\hat{\epsilon}$ and Rademacher complexity of the hypothesis class \mathcal{F} . We can use the classic results from (Ando et al., 2005). Define empirical Rademacher complexity for samples from all tasks as

$$\hat{R}_{\mathbf{X}}(\mathcal{F}) = \mathbb{E}_{\sigma} \left[\sup_{f \in \mathcal{F}} \left(\frac{1}{nK} \sum_{k=1}^K \sum_{i=1}^n \sigma_k^{(i)} l(f(\mathbf{x}_k^{(i)})) \right) \right] \quad (7)$$

where $\{\sigma_k^{(i)}\}$ are independent binary variables $\sigma_k^{(i)} \in \{-1, 1\}$. The true Rademacher complexity is then defined $R(\mathcal{F}) = \mathbb{E}_{\mathbf{X}}(\hat{R}_{\mathbf{X}}(\mathcal{F}))$.

The following theorem restates the main result from (Ando et al., 2005). We simplify the statement by using the Rademacher complexity rather than the set cover number argument used in the original proof.

Theorem B.1. (Ando et al., 2005) *Given data from K different forecasting tasks μ_1, \dots, μ_k and f in hypothesis class \mathcal{F} , for some constant C with probability at least $1 - \delta$, the following inequality holds:*

$$\frac{1}{K} \sum_k \epsilon_k(f) \leq \frac{1}{K} \sum_k \hat{\epsilon}_k(f) + 2R(\mathcal{F}) + C \sqrt{\frac{\log 1/\delta}{nK}}. \quad (8)$$

If we assume the loss is bounded $l \leq 1/2$, then we may take $C = 1/\sqrt{2}$.

Proof. Consider $\{\mathbf{x}_k^{(i)}\}$ as independent random variables. For a function ϕ that satisfies

$$|\phi(\mathbf{x}^{(1)}, \dots, \mathbf{x}^{(i)}, \dots, \mathbf{x}^{(n)}) - \phi(\mathbf{x}^{(1)}, \dots, \tilde{\mathbf{x}}^{(i)}, \dots, \mathbf{x}^{(n)})| \leq c_i$$

by McDiarmid's inequality, we have

$$p\left(\phi(\mathbf{x}^{(1)}, \dots, \mathbf{x}^{(n)}) - \mathbb{E}[\phi] \geq t\right) \leq \exp\left(-\frac{2t^2}{\sum_i c_i^2}\right).$$

Applying this inequality to the max difference $Q(\mathbf{X}) = \sup_{f \in \mathcal{F}} [\epsilon(f) - \hat{\epsilon}(f, \mathbf{X})]$, then with probability at least $1 - \delta$, we have

$$Q(\mathbf{X}) - \mathbb{E}_{\mathbf{X}}[Q(\mathbf{X})] \leq C \sqrt{\frac{\log 1/\delta}{nK}}$$

where C is a constant depending on the bounds c_i . If the loss $l \leq 1/2$, then $|Q| \leq 1/2$ and so we can take $c_i = 1$ leading to $C = 1/\sqrt{2}$. A standard computation (see (Mohri et al., 2018), Theorem 3.3) using the law of total expectation shows $\mathbb{E}_{\mathbf{X}}[Q(\mathbf{X})] \leq 2R(\mathcal{F})$, which finishes the proof. \square

We can use this to compare the generalization error of multi-task learning versus that of learning the individual tasks. The following inequality compares the Rademacher complexity for multi-task learning to that of individual task learning. Denote $\hat{R}_{\mathbf{X}_k}$ and R_k the empirical and true Rademacher complexity for \mathcal{F} over μ_k .

Lemma B.2. *The Rademacher complexity for multi-task learning is bounded $R(\mathcal{F}) \leq (1/K) \sum_{k=1}^K R_k(\mathcal{F})$.*

Proof. We compute the empirical Rademacher complexity,

$$\begin{aligned} \hat{R}_{\mathbf{X}}(\mathcal{F}) &= \mathbb{E}_{\sigma} \left[\sup_{f \in \mathcal{F}} \left(\frac{1}{nK} \sum_{k=1}^K \sum_{i=1}^n \sigma_k^{(i)} l(f(\mathbf{x}_k^{(i)})) \right) \right] \leq \mathbb{E}_{\sigma} \left[\sum_{k=1}^K \sup_{f \in \mathcal{F}} \left(\frac{1}{nK} \sum_{i=1}^n \sigma_k^{(i)} l(f(\mathbf{x}_k^{(i)})) \right) \right] \\ &= \frac{1}{K} \sum_{k=1}^K \mathbb{E}_{\sigma} \left[\sup_{f \in \mathcal{F}} \left(\frac{1}{n} \sum_{i=1}^n \sigma_k^{(i)} l(f(\mathbf{x}_k^{(i)})) \right) \right] \\ &= \frac{1}{K} \sum_{k=1}^K \mathbb{E}_{\sigma_k} \left[\sup_{f \in \mathcal{F}} \left(\frac{1}{n} \sum_{i=1}^n \sigma_k^{(i)} l(f(\mathbf{x}_k^{(i)})) \right) \right] \\ &= \frac{1}{K} \sum_{k=1}^K \hat{R}_{\mathbf{X}_k}(\mathcal{F}) \end{aligned}$$

The first inequality follows from the sub-additivity of the supremum function. The next equality is due to the fact positive scalars commute with supremum, and by the linearity of expectation. The expectation \mathbb{E}_{σ} reduces to the expectation \mathbb{E}_{σ_k} over only those Rademacher variables appearing inside the expectation. $R_k(\mathcal{F})$ is the Rademacher complexity of the function on the individual task k . Taking expectation over all samples \mathbf{X} gives the result. \square

It is instructive to compare the bound from [Theorem B.1](#) with the generalization error bound obtained by considering each task individually.

Proposition B.3. *Assume $n = n_k$ for all tasks k and the loss l is bounded $l \leq 1/2$, then the generalization bound given by considering each task individually is*

$$\epsilon(f) \leq \hat{\epsilon}(f) + 2 \left(\frac{1}{K} \sum_{k=1}^K R_k(\mathcal{F}) \right) + \sqrt{\frac{\log 1/\delta}{2n}}. \quad (9)$$

which is strictly looser than the bound from [Theorem B.1](#) under the same assumptions.

This result helps to explain why our multitask learning framework has better generalization than learning each task independently. The shared data tightens the generalization bound.

Proof. Applying the classical analog of [Theorem B.1](#) to a single task, we find with probability greater than $1 - \delta$,

$$\epsilon_k(f) \leq \hat{\epsilon}_k(f) + 2R_k(\mathcal{F}) + C_k \sqrt{\frac{\log 1/\delta}{n}}.$$

Averaging over all tasks yields

$$\frac{1}{K} \sum_{k=1}^K \epsilon_k(f) \leq \frac{1}{K} \sum_{k=1}^K \hat{\epsilon}_k(f) + 2 \frac{1}{K} \sum_{k=1}^K R_k(\mathcal{F}) + \frac{1}{K} \sum_{k=1}^K C_k \sqrt{\frac{\log 1/\delta}{n}}.$$

Since the loss l is bounded $l \leq 1/2$, we can take $C = C_k = 1/\sqrt{2}$, giving the generalization upper bound for the joint error of [Equation 9](#).

By [Lemma B.2](#) and the fact $1/\sqrt{2nK} \leq 1/\sqrt{2n}$, the bound in [Theorem B.1](#) is strictly tighter. □

B.2. Domain Adaptation Error

Since we test on $c \sim \mathcal{C}$ outside the training set $\{c_k\}$, we incur error due to domain adaptation from the source domains $\mu_{c_1}, \dots, \mu_{c_K}$ to target domain μ_c with μ being the true distribution. Denote the corresponding empirical distributions of n samples per task by $\hat{\mu}_c = \frac{1}{n_c} \sum_{i=1}^{n_c} \delta_{\mathbf{x}_c^{(i)}}$. For different c and c' , the domains μ_c and $\mu_{c'}$ may have largely disjoint support, leading to very high KL divergence. However, if c and c' are close, samples $\mathbf{x}_c \sim \mu_c$ and $\mathbf{x}_{c'} \sim \mu_{c'}$ may be close in the domain \mathcal{X} with respect to the metric $\|\cdot\|_{\mathcal{X}}$. For example, if the external forces c and c' are close, the distance between the velocity fields $\|\mathbf{x}_c - \mathbf{x}_{c'}\|$ may be small. Choosing a measurement between μ_c and $\mu_{c'}$ which depends on the metric in the space \mathcal{X} such as the Wasserstein distance $W_1(\mu_c, \mu_{c'})$ is thus appropriate. The bound from ([Redko et al., 2017](#)) applies well to our setting as such:

Theorem B.4 ([\(Redko et al., 2017\), Theorem 2](#)). *Let $\lambda_c = \min_{f \in \mathcal{F}} (\epsilon_c(f) + 1/K \sum_{k=1}^K \epsilon_{c_k}(f))$. There is $N = N(\dim(\mathcal{X}))$ such that for $n > N$, for any hypothesis f , with probability at least $1 - \delta$,*

$$\begin{aligned} \epsilon_c(f) &\leq \frac{1}{K} \sum_{k=1}^K \epsilon_{c_k}(f) + W_1 \left(\hat{\mu}_c, \frac{1}{K} \sum_{k=1}^K \hat{\mu}_{c_k} \right) \\ &\quad + \sqrt{2 \log(1/\delta)} \left(\sqrt{1/n} + \sqrt{1/(nK)} \right) + \lambda_c. \end{aligned}$$

Proof. We apply ([Redko et al., 2017](#)) Theorem 2 to target domain $\mu_T = \mu_c$ and joint source domain $\mu_S = 1/K \sum_{k=1}^K \mu_{c_k}$ with empirical samples $\hat{\mu}_T = \hat{\mu}_c$ and $\hat{\mu}_S = 1/K \sum_{k=1}^K \hat{\mu}_{c_k}$. □

B.3. Encoder versus Prediction Network Error

Our goal is to learn a joint hypothesis h over the entire domain \mathcal{X} in two steps, first inferring the task c and then inferring x_{t+1} conditioned on c . Error from DyAd may result from either the encoder g_ϕ or the prediction network f_θ . Our hypothesis space has the form $\{x \mapsto f_\theta(x, g_\phi(x))\}$ where ϕ and θ are the weights of the encoder and prediction network respectively.

Let $\epsilon_{\mathcal{X}}$ be the error over the entire domain \mathcal{X} , that is, for all c . Let $\epsilon_{\text{enc}}(g_{\phi}) = \mathbb{E}_{x \sim \mathcal{X}}[\mathcal{L}_1(g(x), g_{\phi}(x))]$ be the encoder error where $g: \mathcal{X} \rightarrow \mathcal{C}$ is the ground truth. We state a result that decomposes the final error into that attributable to the encoder and that to the prediction network.

Proposition B.5. *Assume $c \mapsto f_{\theta}(\cdot, c)$ is Lipschitz continuous with Lipschitz constant γ uniformly in θ . Then we bound*

$$\epsilon_{\mathcal{X}}(f_{\theta}(\cdot, g_{\phi}(\cdot))) \leq \gamma \epsilon_{\text{enc}}(g_{\phi}) + \mathbb{E}_{c \sim \mathcal{C}}[\epsilon_c(f_{\theta}(x, c))] \quad (10)$$

where the first term is the error due to the encoder incorrectly identifying the task and the second term is the error due to the prediction network alone.

The hypothesis in the second term consists of the prediction network combined with the ground truth task label $x \mapsto f_{\theta}(x, g(x))$.

Proof. By the triangle inequality and linearity of expectation,

$$\begin{aligned} \epsilon_{\mathcal{X}}(f_{\theta}(\cdot, g_{\phi}(\cdot))) &= \mathbb{E}_{c \sim \mathcal{C}}[\mathbb{E}_{x \sim \mu_c}[\|f_{\theta}(x, g_{\phi}(x)) - f(x)\|_{\mathcal{Y}}]] \\ &\leq \mathbb{E}_{c \sim \mathcal{C}}[\mathbb{E}_{x \sim \mu_c}[\|f_{\theta}(x, g_{\phi}(x)) - f_{\theta}(x, c)\|_{\mathcal{Y}}]] + \mathbb{E}_{c \sim \mathcal{C}}[\mathbb{E}_{x \sim \mu_c}[\|f_{\theta}(x, c)\|_{\mathcal{Y}} - f(x)\|_{\mathcal{Y}}]]. \end{aligned}$$

By Lipschitz continuity,

$$\leq \mathbb{E}_{c \sim \mathcal{C}}[\mathbb{E}_{x \sim \mu_c}[\gamma \|g_{\phi}(x) - c\|_{\mathcal{C}}]] + \mathbb{E}_{c \sim \mathcal{C}}[\mathbb{E}_{x \sim \mu_c}[\|f_{\theta}(x, c)\|_{\mathcal{Y}} - f(x)\|_{\mathcal{Y}}]],$$

which, since $g(x) = c$ and by linearity of expectation,

$$= \gamma \mathbb{E}_{c \sim \mathcal{C}}[\mathbb{E}_{x \sim \mu_c}[\|g_{\phi}(x) - g(x)\|_{\mathcal{C}}]] + \mathbb{E}_{c \sim \mathcal{C}}[\mathbb{E}_{x \sim \mu_c}[\|f_{\theta}(x, c)\|_{\mathcal{Y}} - f(x)\|_{\mathcal{Y}}]]$$

and by definition of ϵ_{enc} and ϵ_c ,

$$= \gamma \epsilon_{\text{enc}}(g_{\phi}) + \mathbb{E}_{c \sim \mathcal{C}}[\epsilon_c(f_{\theta}(x, c))]$$

as desired. \square

By combining Theorem B.1, Proposition B.5, and Theorem B.4, we can bound the generalization error in terms of the empirical error of the prediction network on the source domains, the Wasserstein distance between the source and target domains, and the empirical error of the encoder.

Let $\mathcal{G} = \{g_{\phi}: \mathcal{X} \rightarrow \mathcal{C}\}$ be the task encoder hypothesis space. Denote the empirical risk of the encoder g_{ϕ} with respect to \mathbf{X} by $\hat{\epsilon}_{\text{enc}}(g_{\phi})$.

Proposition B.6. *Assuming the hypotheses of Theorem B.1, Proposition B.5, and Theorem B.4,*

$$\begin{aligned} \epsilon_{\mathcal{X}}(f_{\theta}(\cdot, g_{\phi}(\cdot))) &\leq \gamma \hat{\epsilon}_{\text{enc}}(g_{\phi}) + \frac{1}{K} \sum_{k=1}^K \hat{\epsilon}_{c_k}(f_{\theta}(\cdot, c_k)) + 2\gamma R(\mathcal{G}) + 2R(\mathcal{F}) \\ &\quad + (\gamma + 1) \sqrt{\frac{\log(1/\delta)}{2nK}} + \sqrt{2\log(1/\delta)} \left(\sqrt{1/n} + \sqrt{1/(nK)} \right) \\ &\quad + \mathbb{E}_{c \sim \mathcal{C}} \left[W_1 \left(\hat{\mu}_c, \frac{1}{K} \sum_{k=1}^K \hat{\mu}_{c_k} \right) + \lambda_c \right]. \end{aligned}$$

Proof. We start with the bound of Proposition B.5,

$$\epsilon_{\mathcal{X}}(f_{\theta}(\cdot, g_{\phi}(\cdot))) \leq \gamma \epsilon_{\text{enc}}(g_{\phi}) + \mathbb{E}_{c \sim \mathcal{C}}[\epsilon_c(f_{\theta}(x, c))]. \quad (11)$$

By Theorem B.1 or (Mohri et al., 2018), Theorem 3.3, we can bound

$$\epsilon_{\text{enc}}(g_{\phi}) \leq \hat{\epsilon}_{\text{enc}}(g_{\phi}) + 2R(\mathcal{G}) + \sqrt{\frac{\log(1/\delta)}{2nK}}. \quad (12)$$

In order to apply Theorem B.1 to the risk ϵ_c and relate it to the empirical risk, we need to first relate the error on the target domain back to the source domain of our empirical samples. By Theorem B.4,

$$\epsilon_c(f_\theta(\cdot, c)) \leq \frac{1}{K} \sum_{k=1}^K \epsilon_{c_k}(f_\theta(\cdot, c_k)) + W_1 \left(\hat{\mu}_c, \frac{1}{K} \sum_{k=1}^K \hat{\mu}_{c_k} \right) + \sqrt{2 \log(1/\delta)} \left(\sqrt{1/n} + \sqrt{1/(nK)} \right) + \lambda_c. \quad (13)$$

Applying Theorem B.1, this is

$$\leq \frac{1}{K} \sum_{k=1}^K \hat{\epsilon}_{c_k}(f_\theta(\cdot, c_k)) + 2R(\mathcal{F}) + \sqrt{\frac{\log 1/\delta}{2nK}} + W_1 \left(\hat{\mu}_c, \frac{1}{K} \sum_{k=1}^K \hat{\mu}_{c_k} \right) + \sqrt{2 \log(1/\delta)} \left(\sqrt{1/n} + \sqrt{1/(nK)} \right) + \lambda_c. \quad (14)$$

Substituting (12) and (14) into (11) gives

$$\begin{aligned} \epsilon_{\mathcal{X}}(f_\theta(\cdot, g_\phi(\cdot))) &\leq \gamma \left(\hat{\epsilon}_{\text{enc}}(g_\phi) + 2R(\mathcal{G}) + \sqrt{\frac{\log(1/\delta)}{2nK}} \right) \\ &\quad + \mathbb{E}_{c \sim \mathcal{C}} \left[\frac{1}{K} \sum_{k=1}^K \hat{\epsilon}_{c_k}(f_\theta(\cdot, c_k)) + 2R(\mathcal{F}) + \sqrt{\frac{\log 1/\delta}{2nK}} \right. \\ &\quad \left. + W_1 \left(\hat{\mu}_c, \frac{1}{K} \sum_{k=1}^K \hat{\mu}_{c_k} \right) + \sqrt{2 \log(1/\delta)} \left(\sqrt{1/n} + \sqrt{1/(nK)} \right) + \lambda_c \right]. \end{aligned}$$

Finally using linearity of the expectation over $c \sim \mathcal{C}$, removing it where there is no dependence on c , and rearranging terms gives the result. \square